*ECS Journal of Solid State Science and Technology*, **6** (7) P435-P439 (2017)
2162-8769/2017/6(7)/P435/5/$37.00 © The Electrochemical Society


# Transfer Printing of Micron-Size Graphene for Photonic Integrated Circuits and Devices

**Leili Abdollahi Shiramin,[a,z] Alexandre Bazin,[a] Steven Verstuyft,[a] Sylvia Lycke,[b] Peter Vandenabeele,[b] Gunther Roelkens,[a] and Dries Van Thourhout[a]**

[a]*Photonics Research Group, Department of Information Technology, Ghent University-IMEC, Ghent 9052, Belgium*
[b]*Raman Spectroscopy Group, Department of Archaeology, Ghent University, B-9000 Ghent, Belgium*

We demonstrate a new printing method for transferring micron-size graphene films to desired sites on a target substrate. After patterning the graphene layer, a photoresist mask is used to realize a suspended graphene-resist stack. This stack is then transferred toward the desired site on the target substrate using a patterned polydimethylsiloxane (PDMS) stamp in a transfer printing tool. The Raman spectra of the transferred graphene films confirm that no defects are introduced in the process. $Si_3N_4$ waveguides with graphene transferred on top exhibit the expected absorption of 0.054 dB/μm. The sheet resistance and contact resistance of graphene transferred on pre-patterned palladium contacts are 398 Ω/sq and 2990 Ω.μm, respectively, comparable to measurements on the original source wafer. These results prove our method enables simple and cost-effective integration of graphene on a semiconductor target wafer, which may expand the application range of graphene for photonics and electronics.
 [DOI: 10.1149/2.0241707jss] 

Manuscript submitted April 18, 2017; revised manuscript received May 12, 2017. Published May 26, 2017.

In recent years, an enormous amount of effort has been devoted to the development of high quality graphene growth, mainly on metal substrates[1–3] but also on dielectric substrates.[4–7] Integrated photonic devices on the other hand are often fabricated by patterning silicon, III-V semiconductors or silicon nitride layers, not compatible with direct graphene growth. Therefore there is a need for transferring graphene or other 2D materials from its original growth substrate to another substrate.[8–11] Thus far, in most cases large size CVD-grown graphene films or individual flakes of exfoliated material are thereby transferred.[12–19] Such an approach might have considerable drawbacks however. It leads to an inefficient use of the graphene film, especially on large scale photonic integrated circuits, requiring only graphene in a small area of the entire circuit. In some cases, e.g. on preprocessed substrates with large topography, it might even be impossible to transfer full films of 2D-materials. Therefore it is essential to develop a method to transfer small patches of graphene to dedicated locations on a target wafer. Though many such techniques have been proposed,[20–22] a scalable approach allowing transfer of graphene patches at a given set of locations on a target wafer substrate has not yet been demonstrated. To date, the methods employed for the transfer of micron-size graphene layers rely on manual processes derived from the conventional wet transfer,[20–22] using home-built tools, and are strongly dependent on the handling skills of the operator. In most cases they are difficult to upscale to full wafer processing.

In this paper, we present a new method that allows transfer of micron-size graphene toward any desired site on a target substrate, relying on a commercially available tool used also in the solar, display and electronics industry[23–25] and more recently also for the transfer of III-V semiconductors on silicon waveguide circuits.[26] We demonstrate the transfer of patterned monolayer CVD graphene from a $Si/SiO_2$ substrate to different types of target substrates including silicon substrates with a planar $SiO_2$ film, $Si_3N_4$ waveguides and palladium (Pd) contacts. Since the transfer is carried out using an automated tool, the graphene quality is not influenced by the operator skills. Hence, our technique allows for a repeatable and high quality graphene transfer. The presented approach has the capability of transferring micron-size graphene films one by one but allows also transferring multiple films in parallel. This property suggests an efficient way for the wafer scale integration of graphene with other optical components in a photonic chip. Moreover, our technique has the advantage of efficient material use. The graphene can be transferred from a densely populated source substrate to a sparsely populated target substrate. In addition, as after preparing them, the graphene coupons are dry, they can be kept on the source wafer for a long time, allowing the reuse of the source wafer to populate multiple target wafers.

[z]E-mail: Leili.AbdollahiShiramin@ugent.be

## Transfer Printing Procedure

The transfer printer (X-Celeprint, model μTP-100) consists of several stages carrying respectively the source sample (a sample with suspended graphene patterns covered by photoresist), the target sample and a cleaning pad (Figure 1). A patterned PDMS stamp fabricated using a patterned silicon substrate as a master mold (see[27] for details on stamp fabrication) is installed on a glass plate and then attached to the stamp holder above the stages. The stage is motorized and has the capability of moving with sub-micrometer accuracy. The different components of the tool were described in detail in Ref. 28.

The alignment of the stamp with the source and target samples is visualized on a camera looking through the transparent stamp and stamp holder. A 3-sigma alignment accuracy of 1.5 μm has been reported for this tool.[29]

Pickup and printing are based on controlling the adhesion between the stamp and the graphene structures. Graphene pieces, henceforth referred to as coupons, with protective photoresist on top can be picked up from the source substrate by moving up the stamp at high speed thus exerting a force on the coupon exceeding the photoresist tether's strength. They are then printed to the target chip and stay attached while releasing the stamp slowly. This leads to a reduced adhesion between the PDMS and the photoresist, which is now lower than the adhesion of the coupon to the target substrate.[26,30,31] The

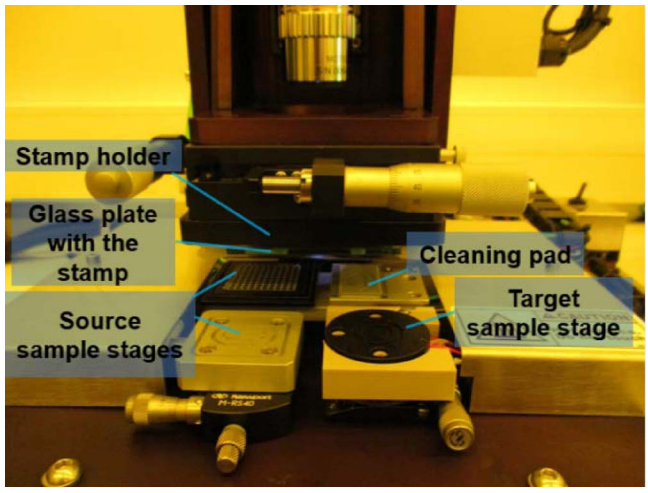


**Figure 1.** The transfer printer machine showing the source sample stage, target sample stage, and cleaning pad. The glass plate with the attached PDMS stamp in the stamp holder is indicated as well.

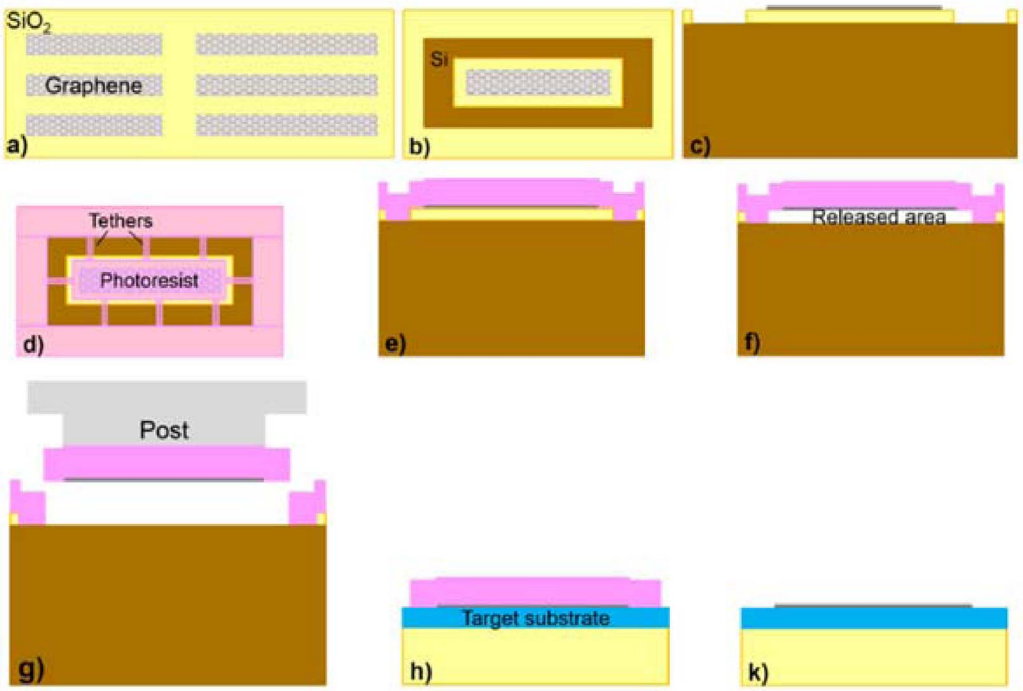


**Figure 2.** Process flow for preparing the source substrate and the actual transfer printing process. a) Top view of array of graphene patterns. b) Top view after $SiO_2$ patterning. c) Side view after $SiO_2$ patterning. d) Top view after tether definition. e) Side view after tether definition. f) Side view after under-etching g) Pickup of the resist-covered graphene coupon h) Resist-covered graphene coupon after printing. k) After resist removal.

tool has a fully automated operation mode whereby the user defines the origin of the first coupon, the horizontal and vertical pitch of the coupons on the source sample, the origin of the first device on the target sample and the pitch between devices on the target sample. From this information the machine is then able to transfer all coupons fully automatically without user intervention. If even higher placement accuracy is required, an additional pattern recognition step with respect to predefined markers on the source and target sample can be added.

The process flow for preparing the source substrate is described in Figure 2. The starting point is a CVD grown graphene film on a 300 nm $SiO_2$ layer on a Si substrate, obtained from Graphenea (www.graphenea.com). First an array of graphene coupons is defined by UV lithography followed by an oxygen plasma, Figure 2a. After patterning, the resist is removed by acetone. Then a trench is etched in the 300 nm $SiO_2$ layer, 10 μm away from the graphene coupons, using a second lithography step, (Figure 2b top view and Figure 2c side view). Following resist removal a new photoresist mask shielding the graphene coupons and forming tethers to the silicon substrate is formed (Figure 2d top view and Figure 2e side view). The used photoresist was TI 35E, a relatively thick resist that can withstand the buffered oxide etch (BOE) needed in the next step. The width of the tethers is a crucial parameter in controlling the under-etch process and avoiding collapse of the coupon while still allowing for easy fracturing during the pick-up process. For $10 \times 250$ $\mu m^2$ graphene coupons, we used 2 μm wide tethers. The next step is to under-etch the sacrificial $SiO_2$ layer in a BOE solution, Figure 2f. To avoid damaging the photoresist during the BOE etch, the sample was baked 5 min at 150°C to harden the photoresist. After under-etching, the sample is gently rinsed by DI water and dried by a nitrogen flow. In this stage, the graphene coupons are suspended by the photoresist tethers and ready for pick-up. Now the source and target samples are loaded in the transfer printer. Figure 2g illustrates the pickup of the graphene coupons protected by photoresist, being attached to the stamp and the tethers breaking as expected. Figures 2h, 2k are images of the graphene transferred to the target device before and after photoresist removal.

The graphene coupons were defined in an array with x-pitch of 400 μm and y-pitch of 60 μm. After a first pick-up and print of a coupon on the target substrate, the stamp moves to the cleaning pad to remove any remaining photoresist or other debris from the stamp. To pick up the next coupon, the stamp is moved back to the source substrate, landing on a second graphene coupon. A new coupon is picked up and printed on the desired spot on the target sample, with a pitch not related to that of the coupons on the source wafer, ensuring economical use of the graphene. In this paper a semi-automatic mode is used, which is identical to the automatic mode described above, except for the fact that for every transfer the source coupon and target location are selected separately in the user interface. The transfer itself, including pick-up and release speeds are fully controlled by the tool, ensuring reliable operation independent of the operator skills. Note that the size of the post on the patterned PDMS stamp should be close to the size of the oxide etch mask shown in Figure 2b to avoid touching neighboring coupons by the stamp. Note that with a suitable stamp design, containing multiple posts, also multiple coupons can be transferred at the same time. This will be demonstrated below.

## Characterization of Transferred Graphene

For preliminary evaluation of the process and the quality of the transferred layers, we transferred graphene to a silicon substrate covered with a 300 nm thick $SiO_2$ layer. Figure 3 shows that the Raman spectrum (532 nm excitation source) of the transferred graphene remains very similar to that of the reference sample. For the reference sample the Full Width at Half Maximum (FWHM) of the 2D and G bands are 34 $cm^{-1}$ and 15 $cm^{-1}$ respectively with $I_{2D}/I_G = 2.170$. For the transferred graphene we found a 2D band FWHM of 30 $cm^{-1}$, a G band FWHM of 16 $cm^{-1}$ and $I_{2D}/I_G = 2.173$ in good agreement with the reference sample. No D band, indicative of defects in the sample is introduced, attesting of the fact that the proposed transfer technique does not degrade the graphene quality. The only difference with the reference sample is that the small peak close to 2400 $cm^{-1}$ in the reference sample is not observed in our measurement. The reason

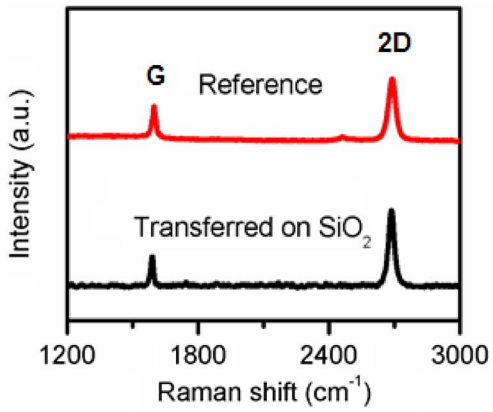


**Figure 3.** The Raman spectrum of a graphene coupon transfer printed on $SiO_2$ compared with the Raman spectrum of the reference sample.

is not fully clear, but it probably relates to the several process steps carried out during the coupon preparation.

In order to demonstrate the possibility of transferring multiple coupons of graphene simultaneously, a stamp with a 2 × 2 pattern of posts is used. It consists of a bulk PDMS layer patterned with 4 posts of 40 × 40 $\mu m^2$ with x-pitch of 250 $\mu$m and y-pitch of 350 $\mu$m (Figure 4a). Figure 4b shows a schematic cross section of the stamp. The pitch of this stamp was chosen to be an integer multiple of the pitch of the graphene coupons on the source wafer, such that in every pick and print operation four graphene coupons are being transferred. We carried out 20 transfer steps (80 graphene coupons total) of which 17 were fully successful. In the other 3 cases at least one of the coupons was not printed. Although not tried here such a failure can in principle be corrected by printing another coupon. Figures 5a and 5b show the transferred graphene coupons before and after removing the protective photoresist. The Raman spectrum in Figure 5c, clearly proves the transfer was successful.

To characterize the optical loss of the printed graphene, we transferred several graphene coupons on planarized silicon nitride waveguides (width = 800 nm, height = 300 nm) with a surface topography of 20 nm, as shown in Figure 6a. Figure 6b shows a magnified image from one of the resulting patterns, showing a clean graphene film covering the waveguide. Figure 6c shows the excess loss of the different graphene covered waveguides with respect to a reference waveguide. The extracted loss of 0.054 dB/$\mu$m is in line with simulations.[32] Figure 6d shows a series of Raman measurements taken at different points

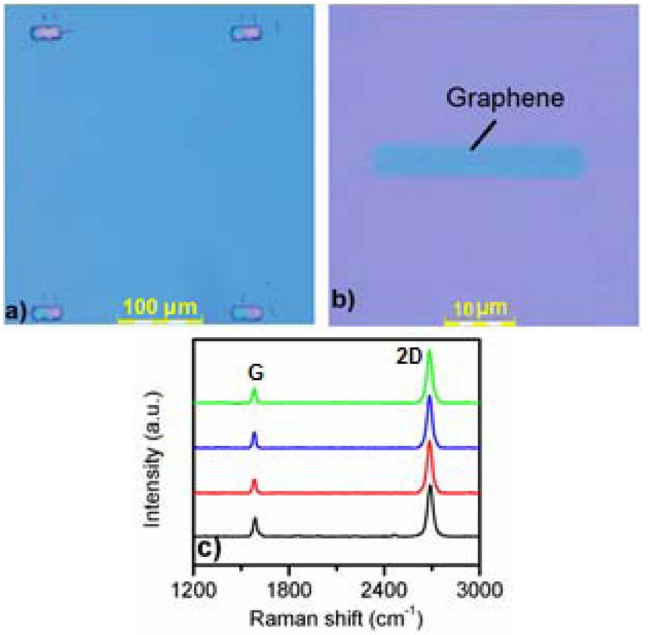


**Figure 5.** a) Microscope picture of 4 resist-covered graphene coupons simultaneously transferred using the stamp shown in Figure 4. b) Zoomed-in image of the graphene after photoresist removal. c) Raman spectra of 4 simultaneously transferred graphene coupons.

on a line orthogonal to the waveguide, starting and ending just outside the rectangular graphene area. Therefore in the recorded spectra, we expect to see peaks associated with monolayer graphene for the central measurement points and no peaks for the outer points (traces number 1 and 10). For the edge traces (number 2 and 9) there is a D band, associated with defects, visible in the spectra. The central traces do not show this band however and for the central trace (number 6) the 2D and G band exhibit a FWHM equal to 33 $cm^{-1}$ and 15 $cm^{-1}$ respectively with $I_{2D}/I_G = 2.36$, again comparable with the reference graphene.

In a final experiment to assess the developed process, we measured the electrical resistivity of transfer printed graphene by two-probe measurement. To this end we defined Pd electrode patterns on a $Si/SiO_2$ substrate using a standard lift-off process. After resist patterning on the target wafer but before metal deposition the $SiO_2$ was slightly etched with BHF such that after the lift-off of Pd the sample

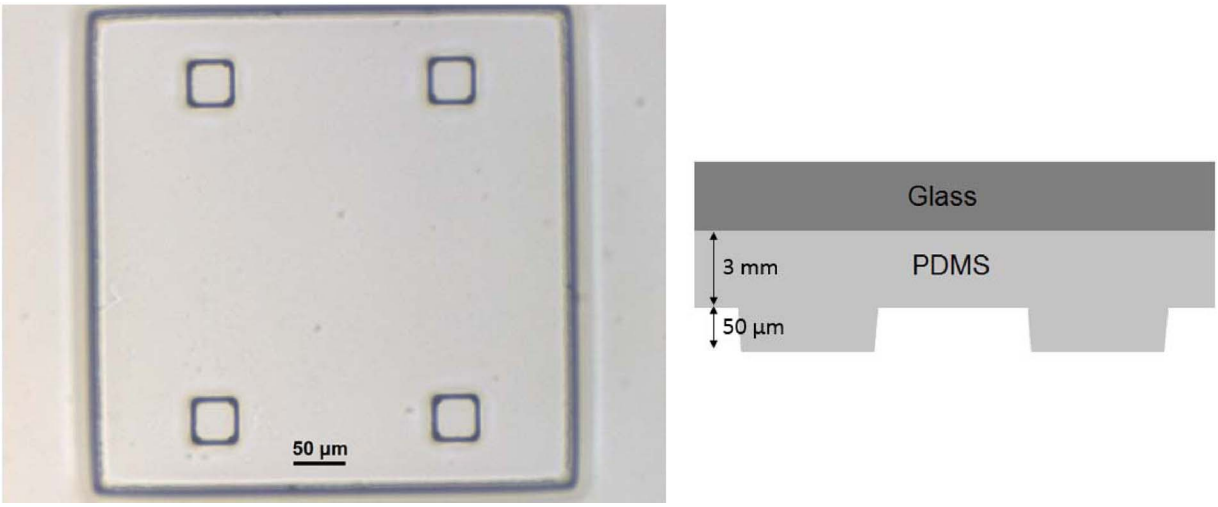


**Figure 4.** a) PDMS-stamp with 4 posts for parallel transfer. b) Schematic cross section of the stamp showing two post in the top part of image a).

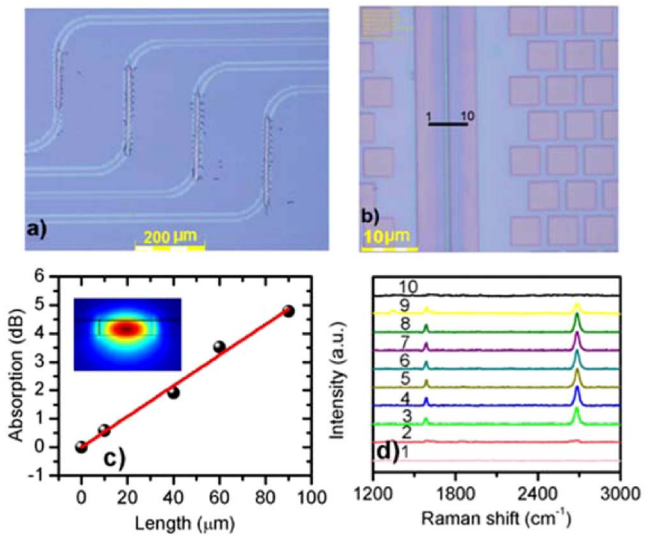


**Figure 6.** a) Resist-covered graphene coupons transferred on $Si_3N_4$ waveguides b) Zoomed-in image after photoresist removal c) Excess loss as function of graphene length. Inset image is the optical mode profile of a graphene integrated $Si_3N_4$ waveguide. d) Raman spectra taken at different points along the line orthogonal with the waveguide as shown in b).

was planarized with a surface topography of 2 nm. Then graphene coupons were transferred on the Pd contacts. Finally the photoresist on top of the graphene was removed. The result, before and after removing the resist is shown in Figures 7a and 7b respectively. The size of the graphene patterns was fixed at 4 × 25 µm$^2$. The contact pad separation was varied from 3 to 25 µm.

The sheet and contact resistance were extracted by applying a voltage between both contacts and measuring the resistance as a function

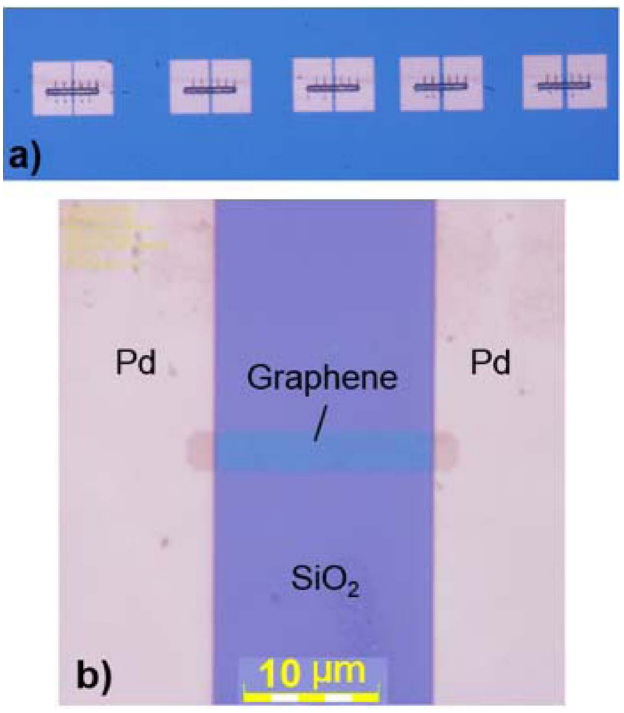


**Figure 7.** a) Transferred graphene sheets on the Pd contact patterns with different contact distance (graphene photoresist encapsulation still present) b) zoomed-in image of graphene on Pd after photoresist encapsulation removal. The distance between contacts is 20 µm.

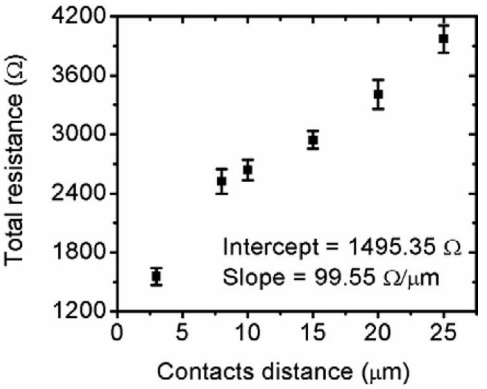


**Figure 8.** Resistance as a function of separation between Pd contacts.

of the contact separation (Figure 8). From the intercept and slope of this curve, the sheet and contact resistance of graphene where found to be 398 Ω/sq and 2990 Ω.µm, respectively. The contact resistance and sheet resistance measured for conventional TLM structures fabricated on samples from the original source wafer are 352 Ω/sq and 928 Ω.µm respectively, similar to other reported values for CVD graphene.[33]

## Conclusions

We presented a new method for transferring multiple micron-size monolayer CVD graphene coupons to a desired site on a target substrate in a reproducible and scalable way using a commercial transfer printing tool (model µTP-100 from X-Celeprint). The processing steps for preparation of the source substrate including graphene patterning, $SiO_2$ etching and the realization of a photoresist encapsulation layer were discussed. The encapsulation layer including tethers that support the free-hanging graphene coupons enables us to release the latter by under-etching the $SiO_2$. The tether size was shown to play an important role in successfully suspending the graphene layers. The pickup and printing speed were optimized to reach a 100% pickup yield and print yield of 95% (in the single coupon transfer). The root cause for the lower print yield is believed to be related to residues originating from the tethers getting underneath the graphene layer. The yield could be improved with further optimization of the tether design ensuring the tethers break such that there is no tether debris underneath the graphene. In addition, an oxygen plasma treatment of the target sample might result in a cleaner target surface and therefore improve the print yield. Raman measurements on the printed graphene coupons and a reference graphene structure indicate the quality of the graphene is preserved after printing. Graphene coupons printed on Pd contact pads allowed us to measure the contact and the sheet resistance of the transferred graphene, which are in line with other reported values for CVD graphene. We believe this work is a large step forward toward the integration of graphene and possibly other 2D-materials on prefabricated photonic integrated circuits and optoelectronic devices such as lasers, modulators and photodiodes on different photonic platforms.

## Acknowledgments

This work was supported by the EU Commission through the H2020 projects TOPHIT and the Graphene Flagship project. We thank C. Huyghebaert, I. Asselberghs and S. Brems for support and useful discussions.

## References

1. H. Wang and G. Yu, *Advanced Materials*, **28**, 4956, (2016).
2. M. Losurdo, M. Michela, P. Capezzuto, and G Bruno, *Phys. Chem. Chem. Phys.*, **13**, 20836, (2011).
3. L. Gao, W. Ren, H. Xu, L. Jin, Z. Wang, T. Ma, L. Ma, Z. Zhang, Q. Fu, L. Peng, X. Bao, and H. Cheng, *Nature Communications*, **3**, 1, (2012).

4. Y. Kim, K. Joo, S. Jerng, J. Lee, E. Yoon, and S. Chun, *Nanoscale*, **6**, 10100, (2014).
5. G. Pan, B. Li, M. Heath, D. Horsell, M. Lesley, L. Taan, and S. Awan, *Carbon.*, **65**, 349, (2013).
6. D. Q. McNerny, B. Viswanath, D. Copic, F. R. Laye, C. Prohoda, A. C. Brieland-Shoultz, E. S. Polsen, N. T. Dee, V. S. Veerasamy, and A. J. Hart, *Scientific Reports*, **4**, (2014).
7. A. Ismach, C. Druzgalski, S. Penwell, A. Schwartzberg, M. Zheng, A. Javey, J. Bokor, and Y. Zhang, *Nano Lett*, **10**(5), 1542, (2010).
8. J. Song, F. Kam, R. Png, W. Seah, J. Zhuo, G. Lim, P. K. H. Ho, and L. Chua, *Nature Nanotechnology*, **8**, 356, (2013).
9. L. Gao, G. Ni, Y. Liu, B. Liu, A. H. Neto, and K. P. Loh, *Nature*, **505**, 190, (2014).
10. J. Kang, D. Shin, S. Bae, and Hong B, *Nanoscale*, **4**, 5527, (2012).
11. A. Castellanos-Gomez, M. Buscema, R. Molenaar, V. Singh, L. Janssen, H. S J. van der Zant, and G. Steele, *2D materials*, **1**, (2014).
12. M. Liu, X. Yin, E. Ulin-Avila, B. Geng, T. Zentgraf, L. Ju, F. Wang, and X. Zhang, *Nature*, **474**, (2011).
13. M. Liu, X. Yin, and X. Zhang, *Nano. Lett.*, **12**, (2012).
14. N. Youngblood, Y. Anugrah, R. Ma, S. J. Koester, and M. Li, *Nano Lett*, **14**, 2741 (2014).
15. Y. Hu, *Laser Photon. Rev.*, **1**, 1, (2016).
16. H. Dalir, Y. Xia, Y. Wang, and X. Zhang, *ACS Photonics*, **3**, (2016).
17. Z. Sun, A. Martinez, and F. Wang, *Nat. Photon.*, **10**, (2016).
18. X. Wang, Z. Cheng, K. Xu, H. Tsang, and J. Xu, *Nat. Photon.*, **7**, (2013).
19. J. Wang, Z. Cheng, Z. Chen, X. Wan, B. Zhu, H. Tsang, C. Shu, and J. Xu, *Nanoscale*, **8**, 13206, (2016).
20. A. Reina, H. Son, L. Jiao, B. Fan, M. S. Dresselhaus, Z. Liu, and J. Kong, *Physical chemistry C*, **112**, 17741, (2008).
21. Y. Bie, Y. Zhou, Z. Liao, K. Yan, S. Liu, Q. Zhao, S. Kumar, H. Wu, G. S. Duesberg, G. L. W. Cross, J. Xu, H. Peng, Z. Liu, and D. Yu, *Advanced Materials*, **23**, 3938, (2011).
22. X. Chen, Z. Liu, W. Jiang, X. Yan, F. ing, P. Wang, Y. Chen, and J. Tian, *Scientific Reports*, **3**, (2013).
23. J. Yoon, S. Jo, I. Chun, I. Jung, H. Kim, M. Meitl, E. Menard, X. Li, J. J. Coleman, U. Paik, and J. A. Rogers, *Nature*, **465**, (2010).
24. S. I. Park, Y. J. Xiong, R. H. Kim, P. Elvikis, M. Meitl, D. H. Kim, J. Wu, J. Yoon, C. J. Yu, Z. J. Liu, Y. G. Huang, K. Hwang, P. Ferreira, X. L. Li, K. Choquette, and J. A. Rogers, *Science*, **325**(5943), 977, (2009).
25. C. Bower, E. Menard, S. Bonafede, J. Hamer, and S. Cok, *IEEE Trans. Compon. Pack. Manufac. Technol.*, **1**, 1916, (2011).
26. A. De Groote, P. Cardile, A. Z. Subramanian, A. M. Fecioru, C. Bower, D. Delbeke, B. Baets, and G. Roelkens, *Optics Express*, **27**, 13754, (2016).
27. D. Gomez, K. Ghosal, A. Meitl, S. Bonafede, C. Prevatte, T. Moore, B. Raymond, D. Kneeburg, A. Fecioru, A. Jose Trindade, and C. A. Bower, *IEEE 66th Electronic Components and Technology Conference.*, (2016).
28. A. Carlson, A. M. Bowen, Y. Huang, R. G. Nuzzo, and J. A. Rogers, *Adv. Mater.*, **24**, 5284, (2012).
29. C. Bower, D. Gomez, K. Lucht, B. Cox, and D. Kneeburg, in *Proceedings of International Display Workshop.*, 1203, (2010).
30. L. A. Meitl, Z. Zhu, V. Kumar, K. Lee, X. Feng, Y. Y. Huang, I. Adesida, R. G. Nuzzo, and J. A. Rogers, *Nat. Mat.*, **5**, 33 (2006).
31. X. Feng, M. A. Meitl, A. M. Bowen, Y. Huang, R. G. Nuzzo, and J. A. Rogers, *Langmuir*, **23**, 12555, (2007).
32. L. Abdollahi Shiramin and D. Van Thourhout, *JSTQE*, **23**, (2017).
33. K. Asadi, *ACS Appl. Mater. Interfaces.*, **7**, 9429 (2015).